pubs.acs.org/acschemicalbiology

Articles

# Photoswitchable Isoprenoid Lipids Enable Optical Control of Peptide Lipidation

Johannes Morstein,[▽] Taysir Bader,[▽] Ariana L. Cardillo,[▽] Julian Schackmann, Sudhat Ashok, James L. Hougland, Christine A. Hrycyna,* Dirk H. Trauner,* and Mark D. Distefano*

Cite This: *ACS Chem. Biol.* 2022, 17, 2945−2953

Read Online

ACCESS | Metrics & More | Article Recommendations | Supporting Information

**ABSTRACT:** Photoswitchable lipids have emerged as attractive tools for the optical control of lipid bioactivity, metabolism, and biophysical properties. Their design is typically based on the incorporation of an azobenzene photoswitch into the hydrophobic lipid tail, which can be switched between its *trans*- and *cis*-form using two different wavelengths of light. While glycero- and sphingolipids have been successfully designed to be photoswitchable, isoprenoid lipids have not yet been investigated. Herein, we describe the development of photoswitchable analogs of an isoprenoid lipid and systematically assess their potential for the optical control of various steps in the isoprenylation processing pathway of CaaX proteins in *Saccharomyces cerevisiae*. One photoswitchable analog of farnesyl diphosphate (**AzoFPP-1**) allowed effective optical control of substrate prenylation by farnesyltransferase. The subsequent steps of isoprenylation processing (proteolysis by either Ste24 or Rce1 and carboxyl methylation by Ste14) were less affected by photoisomerization of the group introduced into the lipid moiety of the substrate a-factor, a mating pheromone from yeast. We assessed both proteolysis and methylation of the a-factor analogs *in vitro* and the bioactivity of a fully processed a-factor analog containing the photoswitch, exogenously added to cognate yeast cells. Combined, these data describe the first successful conversion of an isoprenoid lipid into a photolipid and suggest the utility of this approach for the optical control of protein prenylation.

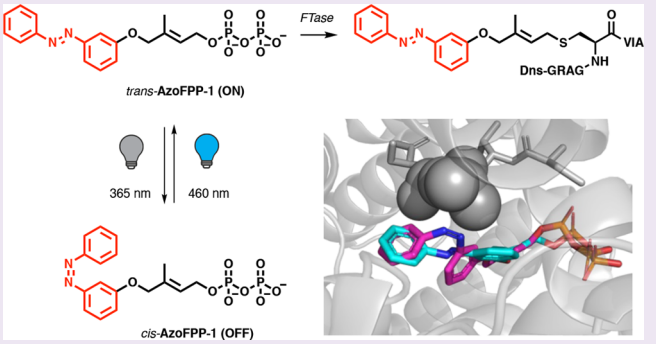


## INTRODUCTION

Approximately 10−20% of all mammalian proteins are thought to undergo protein lipidation.[1] Among the most common types of posttranslational modifications are fatty acylation and isoprenylation.[2] The latter consists of the attachment of an isoprenoid lipid with 3 isoprene repeats (farnesylation, 15 carbons) or 4 isoprene repeats (geranylgeranylation, 20 carbons) by either protein farnesyltransferase (FTase), or types 1, 2, or 3 geranylgeranyltransferase (GGTase I, II, or III) to specific protein substrates. These groups are linked via a thioether bond to one or two cysteine residues positioned near the C-terminus of a target protein.[3] This step is followed by removal of a C-terminal tripeptide sequence by either Ste24 or Ras converting CAAX endopeptidase 1 (RCE1) enzymes,[4,5] and finally methylation of the newly exposed carboxyl cysteine by protein-*S*-isoprenylcysteine *O*-methyltransferase (ICMT).[6] Combined, these modifications generate the functional or active states of the lipidated protein through modulation of its cellular localization or protein−protein interactions.[7]

Several chemical probes have been developed to study and inhibit protein isoprenylation as a means to disrupt the processing of CaaX proteins implicated in disease pathways.[8] Farnesyltransferase inhibitors (FTIs) have been explored in several trials for cancer therapy[9] and have recently been approved for the treatment of hepatitis D virus infections, progeria, and progeroid laminopathies.[10] To allow for improved spatiotemporal control of protein farnesylation, we have previously synthesized FTIs with photocleavable protecting groups that enable the UV-A light-triggered activation of these caged molecules.[11] However, this light-induced inhibition of farnesyltransferase (FTase) is an indirect method to control the function of isoprenylated proteins, and it does not allow for reversibility or activation of the process. We envisioned that reversible control of the structure of the isoprenoid lipid and, in turn, its function could be achieved through the incorporation of a reversibly photoswitchable moiety, such as a hydrophobic azobenzene, into an isoprenoid substrate.

**Received:** August 15, 2022
**Accepted:** September 26, 2022
**Published:** October 4, 2022







https://doi.org/10.1021/acschembio.2c00645
*ACS Chem. Biol.* 2022, 17, 2945−2953

In recent years, this approach has been extensively explored for photoswitchable sphingolipids and glycerolipids.[12] These photolipids have been used to control biological targets of signaling lipids, including GPCRs,[13−15] ion channels,[16−18] enzymes,[19−22] nuclear hormone receptors,[23,24] and immunoreceptors,[25] and as a means to control membrane biophysics in model membranes[26−28] and cells.[29] However, to date, this approach has not been extended to other important classes of lipids, such as steroids or isoprenoids. The development of photoswitchable isoprenoid lipids was further motivated by previously reported arene-rich analogs that proved to be efficient substrates for FTase (Figure 1A).[30] These included a

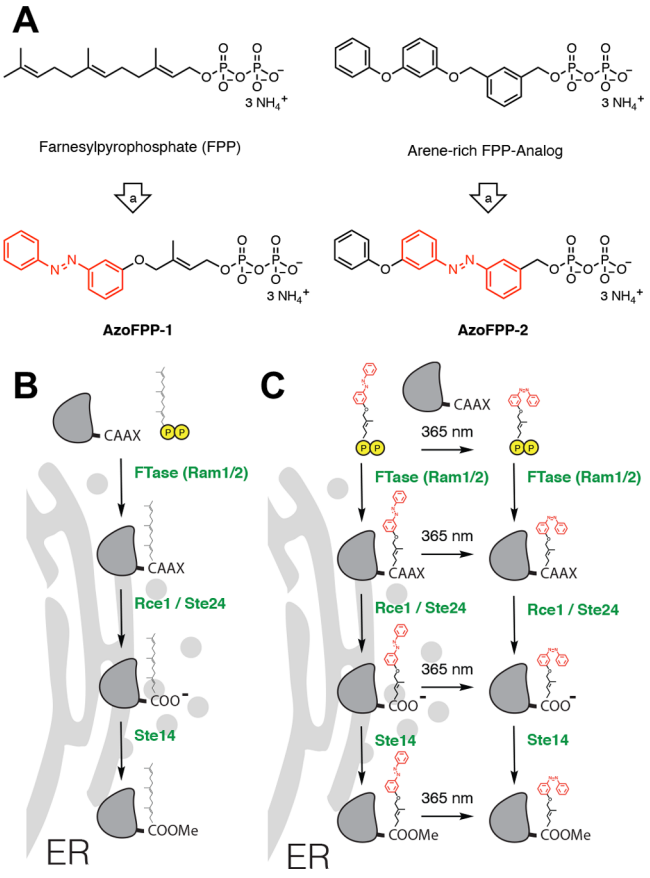


**Figure 1.** Design of photoswitchable FPP analogs and optical probing of prenylation processing. (A) "Azologization" of FPP and arene-rich analog. (B) Schematic illustration of protein farnesylation and subsequent processing. (C) Schematic representation of optical probing of peptide prenylation and processing with photoswitchable FPP analogs.

benzyl phenyl ether, which is a structural isostere ("azostere"[31,32]) of azobenzenes. Photoswitchable analogs could, in principle, allow for optical control of substrate prenylation, processing, and bioactivity (Figure 1B). Herein, we systematically explore the use of photoswitchable farnesyl diphosphate (FPP) analogs, termed **AzoFPP**s, for the optical control of protein isoprenylation, the subsequent processing of isoprenylated peptides, and the bioactivity of a prenylated fully processed, bioactive peptide (Figure 1C). Each enzymatic step in the CaaX pathway was explored with a peptide substrate in either the *trans*- or *cis*-forms to probe the relative sensitivity of lipid structure to the protein isoprenylation processing steps. Lastly, the bioactivity of the mature, fully processed peptide a-factor containing the photoswitchable lipid moiety was assessed using a yeast growth arrest assay. Our results suggest that **AzoFPP**s enable optical control of the isoprenylation step catalyzed by FTases without significantly affecting subsequent processing steps.

## RESULTS AND DISCUSSION

**Design, Synthesis, and Photophysical Characterization of Photoswitchable FPP Analogs.** Initially, two photoswitchable analogs of FPP (Figure 2A) were designed and synthesized (see Figure S1 for the synthetic routes). The first analog, **AzoFPP-1**, was based on directly incorporating an azobenzene into an isoprenoid-like allylic scaffold. The second analog, **AzoFPP-2**, was inspired by a previously reported aryl-FPP derivative developed by Spielmann et al. that showed better steady-state kinetic parameters for isoprenylating an H-Ras sequence compared with FPP, the physiological substrate.[30] This aryl-FPP analog allowed for straightforward azologization[31,32] to obtain a photoswitchable analog. Briefly, 3-hydroxy azobenzene (**2**) was coupled to a prenol-derived alcohol (**1**) via a Mitsunobu reaction, followed by deprotection, which was then transformed into a chloride under Appel conditions.[33] This allowed for the introduction of the diphosphate functionality into **4**. Ion exchange chromatography and further purification gave **AzoFPP-1** (**5**). The azobenzene precursor **6** for **AzoFPP-2** (**7**) was generated under Baeyer−Mills conditions[34,35] followed by a similar reaction sequence to yield the diphosphate (Figure 2A). UV−vis spectroscopy showed that **AzoFPP-1** behaved similarly to an unsubstituted azobenzene (Figure 2B). Isomerization from the thermodynamically favored *trans*-configuration to the *cis*-form was triggered with UV irradiation ($\lambda$ = 365 nm), as evidenced by monitoring via reversed-phase HPLC (Figure S2). This process was reversible using blue light ($\lambda$ = 460 nm) over multiple cycles (Figure 2C). Both compounds underwent slow thermal relaxation to the *trans*-isomer with $t_{1/2}$ = 25 h for **AzoFPP-1** and $t_{1/2}$ = 29 h for **Azo-FPP-2**, measured in PBS buffer at 37 °C.

**Optical Control of Peptide Farnesylation.** Molecular docking studies of the photoswitchable FPP analogs into the structure of *Rattus norvegicus* FTase (rFTase, PDB 1JCR) suggested that the *trans* isomer of the analogs would be accepted by the enzyme better than the *cis* isomer. Notably, we found that *trans*-**AzoFPP-1** (Figure 2E) exhibited a similar binding pose relative to the peptide substrate compared to endogenous FPP (Figure 2D), while *cis*-**AzoFPP-1** exhibited some visible steric clash with leucine of the substrate peptide CVLS, suggesting that this photoisomer may be a less effective substrate for transfer by interfering with the binding of the peptide substrate, the second step in the kinetic mechanism of the enzyme after farnesyl diphosphate (FPP) binding.[36−38]

Based on these promising docking results, the *in vitro* farnesylation of a model peptide (**8a**) with **AzoFPP-1** by yeast farnesyltransferase (yFTase) was explored (Figure 3A, B). The model peptide contained a dansyl fluorophore ($\lambda_{ex}$ = 335 nm; $\lambda_{em}$ = 518 nm) for visualization, an RAG sequence to increase solubility and ionization in mass spectrometry, and a CVIA sequence derived from the precursor to the prenylated yeast mating pheromone a-factor. The ratio of **8a** to the corresponding farnesylated peptide **8b** (with FPP) or **8c**, **d** (with **AzoFPP-1**) was monitored by LC-MS. While the substrate **8a** exhibited a single peak with a retention time of 27.9 min in the absence of enzyme, incubation with yFTase


https://doi.org/10.1021/acschembio.2c00645
ACS Chem. Biol. 2022, 17, 2945−2953

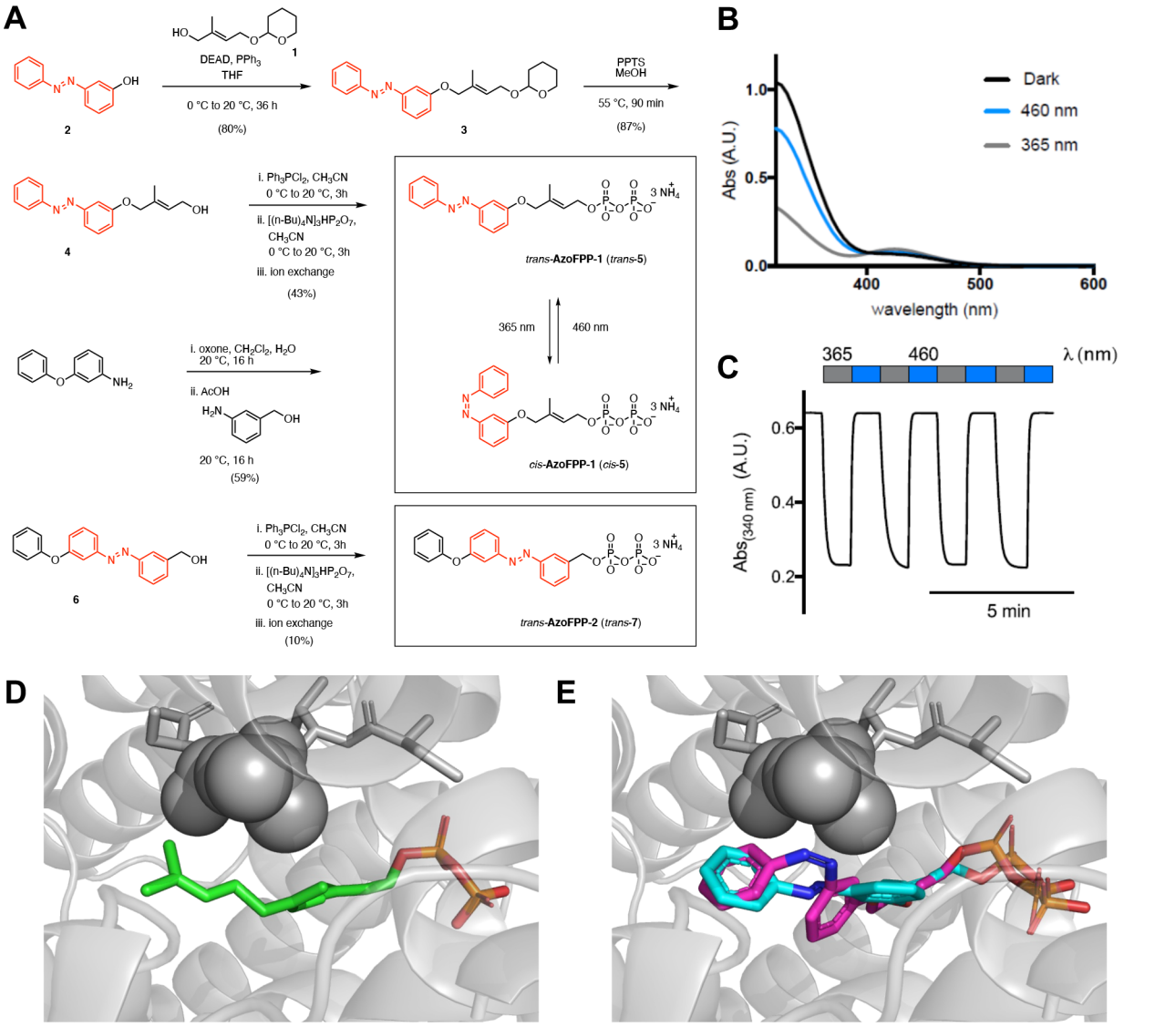


**Figure 2.** Synthesis, photophysical characterization, and molecular docking of photoswitchable farnesyl diphosphate analogs. (A) Chemical synthesis of **AzoFPP-1** and **AzoFPP-2**. (B) The UV−vis spectra of **AzoFPP-1** in varying wavelength-adapted photostationary states were obtained using 50 $\mu$M **AzoFPP-1** in PBS. (C) Reversible cycling between photoisomers with alternating illumination at the two distinct wavelengths, 365 and 460 nm, demonstrated the rapid rate of isomerization. The reactions were performed using 50 $\mu$M **AzoFPP-1** in PBS. (D) Crystal structure of FTase (gray) bound to farnesyl diphosphate (green) and peptide substrate (gray sticks). Spheres are shown for the leucine residue in the CVLS substrate sequence. PDB 1JCR. (E) Molecular docking of **AzoFPP-1** in *trans* (cyan) and *cis* (purple) into FTase. Spheres are shown for the leucine residue in the CVLS substrate sequence.

and FPP resulted in the formation of a new peak with a longer retention time of 58.8 min and a mass consistent with the formation of the farnesylated product **8b** (Figure 3C). Similarly, in the presence of yFTase and **AzoFPP-1**, a new product eluting at 55.1 min with a mass consistent with the formation of **8c** was observed (Figure 3D). At saturating substrate concentrations (22 $\mu$M FPP, 2.4 $\mu$M peptide), 63% of **8a** was converted to **8b**, and this conversion was not significantly affected by irradiation with UV-A light (Figure 3E). For comparison, 51% of **8a** was converted to **8c** under the same conditions with **AzoFPP-1**. Thus, **AzoFPP-1** appears to be an efficient substrate for yFTase, reacting at approximately 80% of the rate observed with FPP. Most importantly, upon irradiation with UV-A light prior to enzyme addition, the conversion to the product was markedly reduced from 51% to 10% (5-fold), demonstrating that *trans*-**AzoFPP-1** undergoes significantly more effective transfer to the peptide substrate allowing for optical control of substrate farnesylation. It is important to note that the reaction mixtures containing **AzoFPP-1** were allowed to relax for 12 h after quenching and prior to analysis; thus, only **8c** was observed and not **8d**. This step simplified the analysis because while **8d** has a distinct retention time that can be detected, it slowly converts to **8c**; allowing complete relaxation eliminated the need to analyze the enzymatic reactions immediately upon completion. To examine whether this marked reduction in rate manifested by *cis*-**AzoFPP-1** was attributable to an effect on $K_M$ or $k_{cat}$, similar experiments were performed at lower isoprenoid concentrations near $K_M$. Under those conditions, *trans*-**AzoFPP-1** again yielded 5-fold greater conversion than *cis*-**AzoFPP-1** (Figure S3). Since the rates measured at high substrate concentration should reflect differences in $k_{cat}$ while the rates


https://doi.org/10.1021/acschembio.2c00645
ACS Chem. Biol. 2022, 17, 2945−2953

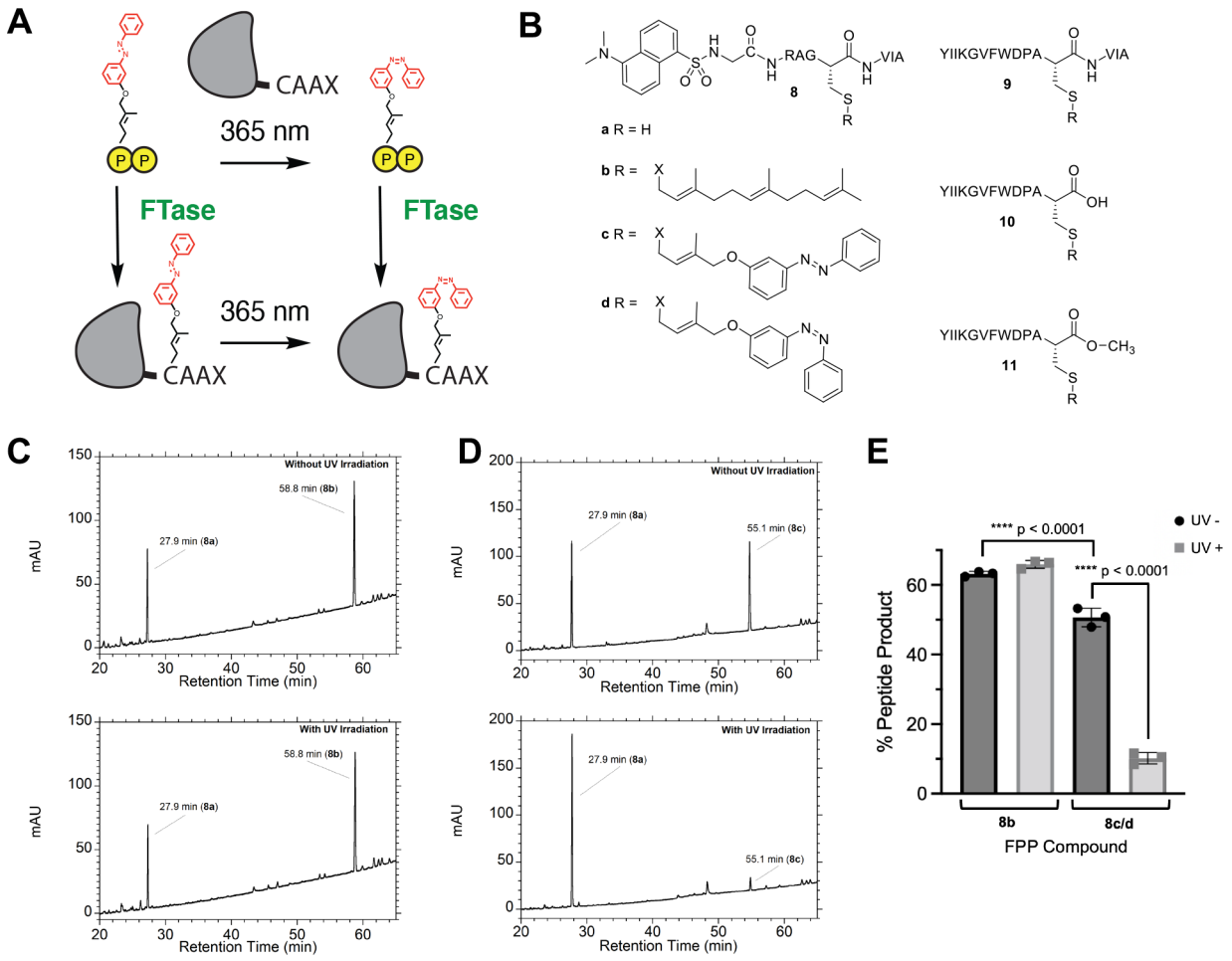


**Figure 3.** Optical control of peptide farnesylation. (A) Schematic representation of model peptide substrate farnesylation with **AzoFPP-1** in the *trans* and *cis* form. (B) Chemical structure of peptide substrate for FTase (**8**) and a-factor variants (**9**–**11**) with various functionalizations (a–d). (C, D) HPLC chromatograms showing conversion of **8a** to **8b** (C) or **8c** (D) upon incubation of **8a** with FPP and yFTase in the dark (top) or after UV-A irradiation (bottom). Substrate concentrations were at saturating levels. Absorbance was monitored at 220 nm. (E) Quantification of panels C and D. Error bars represent SEM.

observed at low substrate concentrations can reflect effects on both $k_{cat}$ and $K_M$, these results suggest that the major impact of isomerization is on $k_{cat}$. Parallel experiments performed with a mammalian farnesyltransferase (*R. norvegicus*, rFTase) exhibited a similar preference for the *trans*-**AzoFPP-1** isomer (Figure S4 and S5). Substrate **AzoFPP-2** did not undergo detectable yFTase- or rFTase-catalyzed transfer to a peptide substrate and was therefore not further pursued in this study.

**Optical Probing of Prenylation Processing.** Given the substantial (5-fold) optical control of the prenyltransferase-catalyzed reaction obtained with **AzoFPP-1**, we then decided to investigate the subsequent steps in the isoprenylation processing pathway, including proteolysis and carboxyl methylation, and the bioactivity of peptides containing the photoswitchable isoprenoid group. For this purpose, the yeast mating pheromone a-factor was employed because it is a well-established substrate for these enzymes, and has a simple bioactive cellular assay. a-Factor has been extensively studied for its three posttranslational modifications (isoprenylation, proteolysis, and carboxyl methylation) that are required for proper mating between two haploid yeast (*S. cerevisiae*) cells.[39−43] a-Factor precursors **9a** and **10a** containing VIA and Cys-COOH C-termini were synthesized by standard solid phase peptide synthetic methods. a-Factor precursor **11a** with a C-terminal methyl ester was prepared using a side chain anchoring methodology where Fmoc-Cys-OMe linked to a trityl resin via its thiol group (Figure S7) was employed for subsequent solid phase peptide synthesis.[44,45] Subsequent peptides were then prenylated chemically with *trans,trans*-farnesyl bromide or the corresponding chloride precursor used to prepare **AzoFPP-1** at pH 5.0 in the presence of $Zn(OAc)_2$ and NaI. These conditions were optimized (Figure S8) based on previously reported procedures.[44−48] Peptides containing a VIA (**9b** and **9c**), Cys-COOH (**10b** and **10c**), or Cys-COMe (**11b** and **11c**) termini were obtained in this manner. Using these model peptides, each processing enzyme was assayed for activity with its respective a-factor substrate in either the *trans*-form (dark) or *cis*-form (after UV-A irradiation) for light-dependent conversion. Compounds **9b** and **9c** were used in experiments with the proteases Rce1 and Ste24, and **10b** and **10c** were utilized with the isoprenylcysteine carboxyl methyltransferase, Ste14, the ICMT from *Saccharomyces cerevisiae* (Figure 4A). To accomplish this, samples were irradiated using our Cell DISCO system[49,50] (75 ms irradiation every 15 s at 370 nm). Generally, azobenzene-containing peptides were converted to products at rates similar to their farnesylated counterpart in each of the enzymatic steps studied, except in the case of Rce1 where a 2-fold decrease was


https://doi.org/10.1021/acschembio.2c00645
ACS Chem. Biol. 2022, 17, 2945−2953

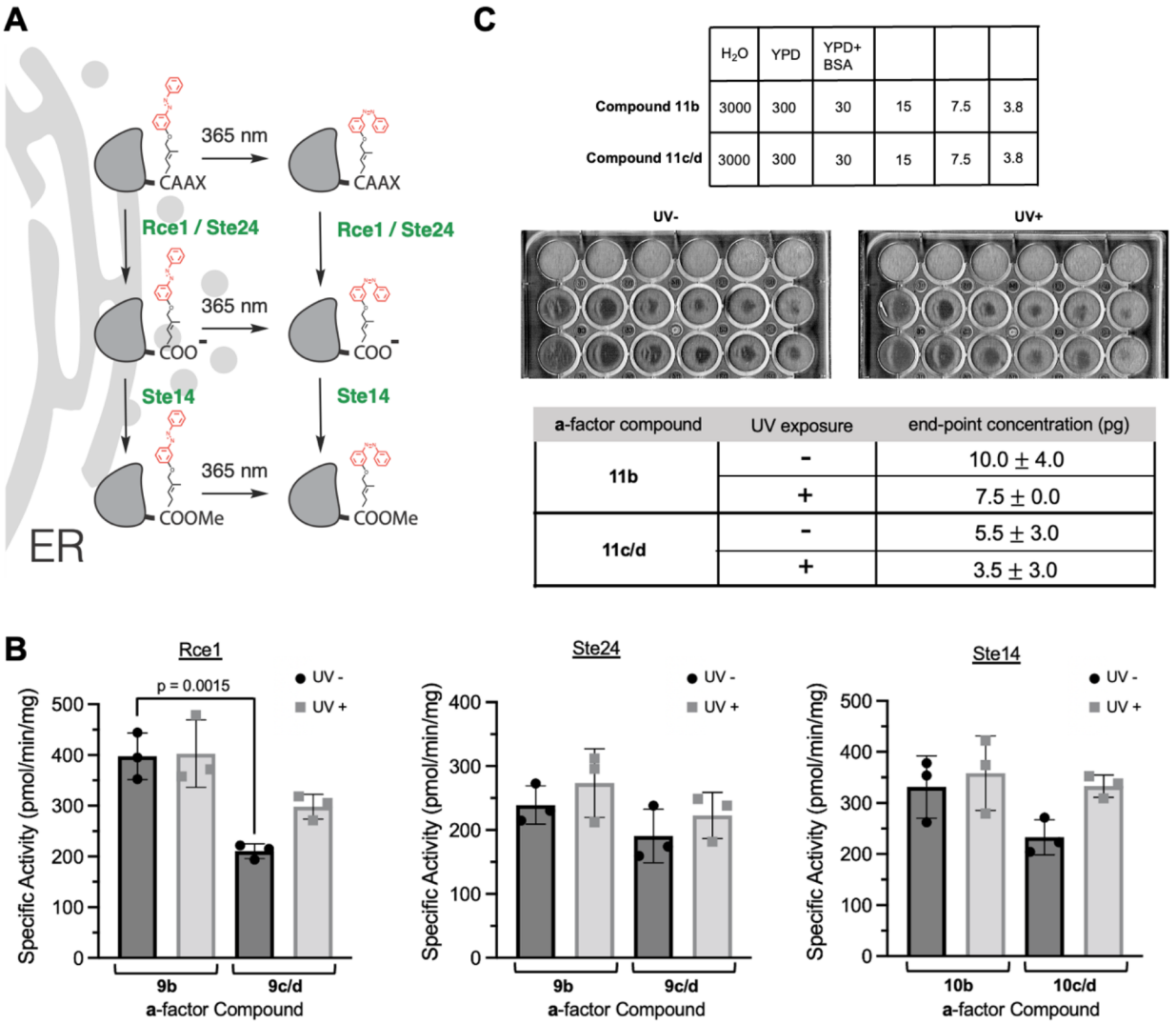


**Figure 4.** Optical probing of prenylation processing pathway. (A) Schematic representation of prenylation processing with photoswitchable a-factor analogs in the *trans* and *cis* form. (B) Quantification with and without UV-A irradiation of Rce1 and Ste24 activity with compounds **9b** and **9c,d** (15 $\mu$M), and Ste14 activity with compounds **10b** and **10c,d** (25 $\mu$M). (C) Yeast growth arrest halo assay with and without UV-A irradiation of compounds **11b** and **11c,d**. The amount of substrate spotted is listed in the table above with solution controls, dd$H_2O$, YPD, and the YPD/BSA mixture used to dilute and make the compound solution, which are in the first row. Quantified growth end-point values are listed in the table below. Error bars represent SEM.

observed with the photolipid-containing peptide (Figure 4B). Each enzyme exhibited only minimal light-dependent activity differences when treated with saturating concentrations of substrate (Figure 4B). These enzymes were further tested at substrate concentrations nearer to the $K_M$ to test for possible $K_M$ effects, such as changes in binding affinity between the two isoprenoid conformations (Figure S8). No significant differences were observed, suggesting that cis/trans isomerization of the diazo-arene had little effect on these enzymatic transformations.

Finally, the bioactivity of the "fully processed" peptides **11b** (a-factor), **11c**, and **11d** was assessed in a yeast growth arrest halo assay employing the DISCO system adapted to a 24-well format (Figure 4C).[42,51] All three peptides were found to be active in this receptor-mediated growth arrest assay and exhibited similar potencies. These data suggest that the bioactivity of a-factor is not sensitive to the structural prenyl-group variations explored. Overall, the optical probing of the prenylation processing pathway reported here suggests that the photoswitchable analog permits selective control of peptide lipidation by farnesyltransferase but exhibits little effect on the subsequent processing steps.

**Concluding Remarks.** Here, we show that isoprenoid lipids can be modified to contain a molecular photoswitch to function as photoswitchable substrates for peptide lipidation by farnesyltransferase. This work enlarges the classes of lipids that can be modified with photoswitches to isoprenoids, which have not been previously investigated using this approach.[12,52] The development of the photoswitchable FPP analog **AzoFPP-1** and its integration into a series of photoswitchable a-factor analogs enabled us to systematically test the utility of these compounds for optical control of various steps in the CaaX processing pathway, including protein isoprenylation, proteolytic processing, carboxyl methylation, and a-factor bioactivity. This study demonstrated that peptide lipidation with **AzoFPP-1** could be effectively modulated through switching between its *trans* and *cis* form, while proteolysis, carboxymethylation, and bioactivity were not sensitive to photoisomerization. These


https://doi.org/10.1021/acschembio.2c00645
ACS Chem. Biol. 2022, 17, 2945−2953

findings suggest that the initial lipidation step is more tightly controlled by lipid structure than the subsequent processing steps and that the tool developed here enables selective optical control of this initial step. Given the importance of isoprenylated proteins in signal transduction pathways, these photoswitchable isoprenoids could be particularly useful for decelerating protein prenylation in a temporally controllable manner or for probing cellular signaling processes that sense or are tightly controlled by isoprenoid structure.[3,53,54]

To date, 2213 isoprenoid lipids have been described (LIPID MAPS[55,56]). Many of these exhibit linear isoprenoid chains that could be functionalized with an azobenzene in an analogous fashion to yield optical control of their function. Linear isoprenoid lipids with interesting bioactivity include the tocotrienols (Vitamin E),[57] cannabinoids (cannabigerol or cannabigerolic acid),[58] the moenomycin antibiotics,[59] or other natural products such as auraptene and umbelliprenin.[60] Isoprenoid lipids have further been used in the design of synthetic pharmacophores, such as the Ras inhibitor salirasib.[61,62] Future efforts will address the development of photoswitchable isoprenoids based on these and other bioactive metabolites to assess how modular the described approach is for the class of isoprenoid lipids.

## MATERIALS AND METHODS

**Photophysical Characterization of AzoFPP-1 and AzoFPP-2.** UV−vis spectra were recorded using a Varian Cary 50 Bio UV−visible spectrophotometer. Photoswitching was achieved using 365 or 460 nm LED light sources. The LEDs were pointed directly onto the top of the sample cuvette with photoswitch (50 $\mu$M in DMSO). An initial spectrum was recorded (dark-adapted state, black) and then again following illumination at 365 nm for 30 s (*cis*-adapted state, gray). A third spectrum was recorded after irradiation at 470 nm for 30 s (*trans*-adapted state, blue). Absorption at 340 nm was recorded over several switching cycles while alternating illumination at 365 and 460 nm.

**Molecular Docking.** For modeling of **AzoFPP-1** in *cis* and *trans* confirmations into the active site of PFTase (pdb file 1JCR), docking was performed using MacroModel v #9.9 and its program Glide. The FTase crystal structure was prepared and minimized using the default settings in the protein preparation wizard as part of the Maestro (Schrodinger Release 2021-03, Maestro Version 12.9.137) package. Prime function was used to fill in missing loops and side chains. Afterward, a receptor grid large enough to encompass the entire binding site for **AzoFPP-1** was generated from the prepared PFTase enzyme. An extra precision docking parameter was set, and 10 000 ligand poses per docking were run per **AzoFPP-1** confirmation. The conformations with the overall highest binding score were chosen for display here.

**yFTase Mediated Prenylation of Peptide dns-CVIA with AzoFPP-1 and AzoFPP-2.** yFTase was expressed and purified as previously described.[63,64] To test if yFTase would process **AzoFPP-1**, a solution of 2.4 $\mu$M **8a** was prepared in yFTase prenylation buffer (50 mM Tris pH 7.5, 15 mM DTT, 10 mM $MgCl_2$, 50 $\mu$M $ZnCl_2$, 20 mM KCl) along with either **AzoFPP-1** or **AzoFPP-2** at 22 $\mu$M and placed in a low-adhesion microcentrifuge tube. Afterward, the enzymatic reactions were initiated by adding yFTase to a final enzyme concentration of 0.100 $\mu$M and a final volume of 250 $\mu$L, then incubating at RT for 20 h. The reactions were quenched by the addition of 50 $\mu$L of glacial $CH_3COOH$ before subjecting to them LCMS analysis. LCMS analysis was performed on an Agilent 1200 series system (Windows 10, ChemStation Software, G1322A Degasser, G1312A binary pump, G1329A autosampler, G1315B diode array detector, 6130 quadrupole) equipped with a C18 column (Agilent ZORBAX 300-SB-C18, 5 $\mu$M, 4.6 mm × 250 mm). Samples were not filtered as filtration caused the observation of no peptide products.

**Kinetic Analysis to Determine Reactivity of *trans*- and *cis*-AzoFPP-1 with yFTase.** A solution of 2.4 $\mu$M **8a** was prepared in yFTase prenylation buffer along with either farnesyl diphosphate (FPP) or **AzoFPP-1** at 22 $\mu$M (high concentration) or 1 $\mu$M (low concentration). UV irradiation of select samples was done by placing the solution in round quartz tubes (10 mm × 50 mm) with 1 mm wall thickness and irradiating in a Rayonet reactor using 3 × 350 nm bulbs (14 W, RPR-3500 Å) for 2 min. To confirm that **AzoFPP-1** was completely isomerized after 2 min and had not relaxed within the time frame required to carry out the enzymatic reaction, a solution containing only **AzoFPP-1** at 22 $\mu$M in prenylation buffer was analyzed by LCMS before and after irradiation with incubation at RT for 1 h. A complete shift in retention time was observed (Figure S2). Afterward, the enzymatic reactions were carried out in low-adhesion microcentrifuge tubes and initiated by adding yFTase to a final enzyme concentration of 0.175 $\mu$M and a final volume of 450 $\mu$L, then incubating at RT for 15 min. The reactions were quenched by the addition of 50 $\mu$L of glacial $CH_3COOH$ before subjecting them to LCMS analysis. LCMS analysis was performed on an Agilent 1200 series system (Windows 10, ChemStation Software, G1322A Degasser, G1312A binary pump, G1329A autosampler, G1315B diode array detector, 6130 quadrupole) equipped with a C18 column (Agilent ZORBAX 300-SB-C18, 5 $\mu$M, 4.6 mm × 250 mm). Samples were not filtered as filtration again caused the observation of no peptide products. All reactions were run in triplicate. The extent of enzymatic conversion was determined by the integration of the starting material and product peaks in 220 nm absorbance chromatograms. This assumes that **8a** and **8c** have a similar $\varepsilon_{220}$ since all the amide bonds as well as the dansyl group exhibit absorbance at that wavelength. To confirm the validity of this assumption, a master mix containing all the reaction components except the enzyme was prepared (2.4 $\mu$M **8a**, 22 $\mu$M, 50 mM Tris pH 7.5, 15 mM DTT, 10 mM $MgCl_2$, 50 $\mu$M $ZnCl_2$, 20 mM KCl). This solution was split into two equal aliquots placed in two low-adhesion microcentrifuge tubes. One aliquot received yFTase enzyme in Tris buffer to a final concentration of 0.175 $\mu$M and a final volume of 450 $\mu$L, while the other received an equal volume of only Tris buffer. After incubating at RT until ∼50% conversion was observed each solution received 50 $\mu$L of glacial $CH_3COOH$ and both were subjected to LC-MS analysis. The integrated 220 nm absorbance of the **8a** peak in the case of the no enzyme solution was 1765.3 units, while the sum of the integrated areas of **8a** and **8c** peaks was 1735.2 units in the case of the sample with yFTase enzyme, which are within 2% of each other.

**rFTase Mediated Prenylation of Peptide dns-CVIS with AzoFPP-1 and AzoFPP-2.** To ascertain if mammalian FTase would process **AzoFPP-1** and **AzoFPP-2**, *Rattus norvegicus* FTase (rFTase) was expressed and purified as previously described.[65,66] dns-CVLS peptide, representing the native sequence of the enzyme with the addition of a dansyl fluorophore for detection and quantification, was incubated at 3 $\mu$M in an rFTase prenylation buffer (50 mM HEPPSO-NaOH, pH 7.8, 5 mM TCEP, and 5 mM MgCl2) (50 $\mu$L total) for 20 min in 0.65 mL low-adhesion Eppendorf tubes. Enzyme solution (50 $\mu$L) containing 100 nM rFTase and 10 $\mu$M **AzoFPP-1** or **AzoFPP-2** was then incubated at RT for 16 h before adding an equal volume of 20% $CH_3COOH$ in $(CH_3)_2CHOH$ and subjecting it to HPLC analysis. HPLC analysis was performed at ambient temperature on an Agilent 1260 HPLC system with autosampler and UV−vis and fluorescence detection using a C18 reversed-phase analytical column (Zorbax XDB-C18). A linear gradient from 30% acetonitrile in 25 mM ammonium acetate to 100% acetonitrile flowing at 1 mL/min over 30 min was used. Peptides and products were detected by fluorescence ($\lambda_{ex}$ 340 nm, $\lambda_{em}$ 496 nm). In the case of **AzoFPP-1**, complete conversion was observed. In the case of **AzoFPP-2**, no conversion was observed (data not shown).

**Kinetic Analysis to Determine Reactivity of *trans*- and *cis*-AzoFPP-1 with rFTase.** To test if there would be a difference in the rate of processing of *trans*-**AzoFPP-1** vs *cis*-**AzoFPP-1** by rFTase, solutions of 3 $\mu$M dns-GCVLS peptide in rFTase prenylation buffer were incubated for 20 min in 0.65 mL low-adhesion Eppendorf tubes. These solutions were then either nonilluminated (trans-isomer) or


https://doi.org/10.1021/acschembio.2c00645
ACS Chem. Biol. 2022, 17, 2945−2953

illuminated with 365 nm LED light (cis isomer) for 3 min in the dark. To initiate the reaction, 50 μL solutions containing 100 nM rFTase and 10 μM **AzoFPP-1** in rFTase prenylation buffer were added to each tube. Reactions were incubated at RT for different time points, 30, 60, 120, 240, or 360 min, before quenching and running HPLC analysis as described above. Reaction progress, expressed as % conversion, was calculated by dividing the product integral by the sum of the product and substrate integrals followed by my multiplication by 100.

**Growth Arrest Assay.** Growth arrest assays were performed as previously described with modifications.[42,51] Briefly, supersensitive, *ss2* MATα cells (strain SM2375) were grown overnight at 30 °C in yeast peptone dextrose (YPD) media. Cells were pelleted at 2000*g*, washed twice with $ddH_2O$ prior to resuspension in $ddH_2O$ at $1 \times 10^6$ cells/mL, and combined with Bacto agar (1.1% in YPD) for a final concentration of 250 000 cells/mL. Cells were spread onto solid YPD medium in each well of a 24-well plate to form a lawn of MATα cells at 20 000 cells/well. Dilutions of FPP (**11b**) and **AzoFPP-1** (**11c,d**) a-factor analogs were prepared in 0.5% bovine serum albumin (BSA)/YPD. UV-treated samples were irradiated for 2 min at 365 nm. For all samples, 2.5 μL of diluted a-factor analog were spotted onto the lawn in 3000, 300, 30, 15, 7.5, and 3.8 pg amounts. Plates were incubated for 24 h at 30 °C in the dark or under UV-A irradiation using the Cell DISCO system (5 ms irradiation every 15 s at 370 nm).[49,50] The assay endpoint was determined for each a-factor analog and UV treatment condition to be the lowest concentration at which agar clearance was detectable. Each experiment was performed in triplicate.

**Protease and Methyltransferase Assays.** Proteolytic and methylation assays were performed using crude membrane preparations as previously described.[6,67,68] Briefly, proteolysis by Rce1 and Ste24 was measured using a coupled proteolysis/methylation assay in which crude membrane preparations from *S. cerevisiae* overexpressing Rce1 or Ste24 (5 μg) were combined with excess amounts of Ste14 overexpressing crude membranes (10 μg per condition). FPP (**9b**) or **AzoFPP-1** (**9c,d**) a-factor analogs were assayed at saturating (maximal velocity, $V_{max}$) conditions of 15 μM (Figure 4B). These compounds were also tested below established $K_M$ values for the enzymes (Figure S7).[42] Samples were preirradiated with UV-A (370 nm) light for 2 min. Subsequently, 20 μM *S*-adensoyl [$^{14}$C-methyl]-L-methionine (52.6 mCi/mmol) (PerkinElmer, USA) in 100 mM Tris-HCl, pH 7.5, was added to the reaction. Reactions were incubated at 30 °C for 30 min under dark or UV-A conditions using the Cell DISCO, as described above. Reactions were terminated with the addition of 50 μL of 1 M NaOH/1% SDS. Reaction mixtures were spotted onto filter paper, which was placed in the neck of a closed vial above 10 mL of scintillation fluid. [$^{14}$C]-methanol vapors were allowed to diffuse into the scintillation fluid for 3 h at RT and subsequently quantified by liquid scintillation counting. Sample counts were corrected using background in the absence of enzyme. For the evaluation of methylation by Ste14, similar conditions were used, with FPP (**10b**) or **AzoFPP-1** (**10c,d**) a-factor analogs at saturating (maximal velocity, $V_{max}$) conditions of 25 μM (Figure 4B).[42] Substrate (5 μM) was used for conditions below $K_M$ of Ste14 (Figure S7). Each reaction was performed in duplicate and counted three times. Assays were repeated in triplicate. Enzyme specific activity is reported as picomoles of methyl groups transferred per minute per milligram of enzyme.

## ■ ASSOCIATED CONTENT

### Supporting Information

The Supporting Information is available free of charge at https://pubs.acs.org/doi/10.1021/acschembio.2c00645.

Supplementary Figures, experimental procedures and compound characterization including $^1$H NMR, $^{13}$C NMR, and $^{31}$P NMR spectra and HPLC chromatograms (PDF)

## ■ AUTHOR INFORMATION


### Corresponding Authors

**Christine A. Hrycyna** − *Department of Chemistry, Purdue University, West Lafayette, Indiana 47907, United States;* orcid.org/0000-0001-9881-2063; Email: hrycyna@purdue.edu

**Dirk H. Trauner** − *Department of Chemistry, New York University, New York, New York 10003, United States; Department of Chemistry, University of Pennsylvania, Philadelphia, Pennsylvania 19104, United States;* orcid.org/0000-0002-6782-6056; Email: dtrauner@upenn.edu

**Mark D. Distefano** − *Department of Chemistry, University of Minnesota, Minneapolis, Minnesota 55455, United States;* orcid.org/0000-0002-2872-0259; Email: diste001@umn.edu

### Authors

**Johannes Morstein** − *Department of Cellular and Molecular Pharmacology and Howard Hughes Medical Institute, University of California, San Francisco, California 94158, United States; Department of Chemistry, New York University, New York, New York 10003, United States;* orcid.org/0000-0002-6940-288X

**Taysir Bader** − *Department of Chemistry, University of Minnesota, Minneapolis, Minnesota 55455, United States;* orcid.org/0000-0002-0682-1905

**Ariana L. Cardillo** − *Department of Chemistry, Purdue University, West Lafayette, Indiana 47907, United States;* orcid.org/0000-0002-9770-2177

**Julian Schackmann** − *Department of Chemistry, New York University, New York, New York 10003, United States*

**Sudhat Ashok** − *Department of Chemistry, Syracuse University, Syracuse, New York 13244, United States*

**James L. Hougland** − *Department of Chemistry, Syracuse University, Syracuse, New York 13244, United States; Department of Biology and BioInspired Syracuse: Institute for Material and Living Systems, Syracuse University, Syracuse, New York 13244, United States;* orcid.org/0000-0003-0444-1017

Complete contact information is available at: https://pubs.acs.org/10.1021/acschembio.2c00645


### Author Contributions

[▽]J.M., T.B., and A.L.C. contributed equally. J.M., T.B., A.L.C., J.S., and S.A. performed experiments. J.M., T.B., A.L.C., J.S., and S.A. analyzed data. J.M., C.A.H., D.H.T., and M.D.D. conceived the study. J.L.H., C.A.H., D.H.T., and M.D.D. supervised the study. J.M. wrote the first draft. T.B., A.L.C., C.A.H., D.H.T., and M.D.D. revised the manuscript. All authors commented on the manuscript.

### Notes

The authors declare no competing financial interest.

## ■ ACKNOWLEDGMENTS

J.M. thanks the NCI for a K00 award (K00CA253758). J.L.H. thanks the NIH for funding (R01GM132606). D.T. thanks the National Institutes of Health for financial support (R01NS108151). M.D.D. and C.A.H. thank the National Science Foundation for funding (NSF/CHE 1905204). The authors thank Ian M. Ahearn and Mark R. Philips for their

helpful comments and experimental support in the early stages of this study.

## REFERENCES

(1) Khoury, G. A.; Baliban, R. C.; Floudas, C. A. Proteome-Wide Post-Translational Modification Statistics: Frequency Analysis and Curation of the Swiss-Prot Database. *Sci. Rep.* **2011**, *1* (1), 90.
(2) Jiang, H.; Zhang, X.; Chen, X.; Aramsangtienchai, P.; Tong, Z.; Lin, H. Protein Lipidation: Occurrence, Mechanisms, Biological Functions, and Enabling Technologies. *Chem. Rev.* **2018**, *118* (3), 919−988.
(3) Wang, M.; Casey, P. J. Protein Prenylation: Unique Fats Make Their Mark on Biology. *Nat. Rev. Mol. Cell Biol.* **2016**, *17* (2), 110−122.
(4) Ma, Y. T.; Chaudhuri, A.; Rando, R. R. Substrate Specificity of the Isoprenylated Protein Endoprotease. *Biochemistry* **1992**, *31* (47), 11772−11777.
(5) Ashby, M. N.; King, D. S.; Rine, J. Endoproteolytic Processing of a Farnesylated Peptide in Vitro. *Proc. Natl. Acad. Sci. U. S. A.* **1992**, *89* (10), 4613−4617.
(6) Hrycyna, C. A.; Clarke, S. Farnesyl Cysteine C-Terminal Methyltransferase Activity Is Dependent upon the STE14 Gene Product in Saccharomyces Cerevisiae. *Mol. Cell. Biol.* **1990**, *10* (10), 5071−5076.
(7) Gelb, M. H.; Brunsveld, L.; Hrycyna, C. A.; Michaelis, S.; Tamanoi, F.; Van Voorhis, W. C.; Waldmann, H. Therapeutic Intervention Based on Protein Prenylation and Associated Modifications. *Nat. Chem. Biol.* **2006**, *2* (10), 518−528.
(8) Palsuledesai, C. C.; Distefano, M. D. Protein Prenylation: Enzymes, Therapeutics, and Biotechnology Applications. *ACS Chem. Biol.* **2015**, *10* (1), 51−62.
(9) Pass, W. FTase Inhibition Holds Promise for RAS Targeting and Beyond*Oncology Live*. 2018, https://www.onclive.com/view/ftase-inhibition-holds-promise-for-ras-targeting-and-beyond.
(10) Dhillon, S. Lonafarnib: First Approval. *Drugs* **2021**, *81* (2), 283−289.
(11) Abate-Pella, D.; Zeliadt, N. A.; Ochocki, J. D.; Warmka, J. K.; Dore, T. M.; Blank, D. A.; Wattenberg, E. V.; Distefano, M. D. Photochemical Modulation of Ras-Mediated Signal Transduction Using Caged Farnesyltransferase Inhibitors: Activation by One- and Two-Photon Excitation. *ChemBioChem* **2012**, *13* (7), 1009−1016.
(12) Trauner, D.; Morstein, J. Optical Control of Glycerolipids and Sphingolipids. *Chimia* **2021**, *75* (12), 1022−1025.
(13) Frank, J. A.; Yushchenko, D. A.; Fine, N. H. F.; Duca, M.; Citir, M.; Broichhagen, J.; Hodson, D. J.; Schultz, C.; Trauner, D. Optical Control of GPR40 Signalling in Pancreatic $\beta$-Cells. *Chem. Sci.* **2017**, *8* (11), 7604−7610.
(14) Morstein, J.; Hill, R. Z.; Novak, A. J. E.; Feng, S.; Norman, D. D.; Donthamsetti, P. C.; Frank, J. A.; Harayama, T.; Williams, B. M.; Parrill, A. L.; Tigyi, G. J.; Riezman, H.; Isacoff, E. Y.; Bautista, D. M.; Trauner, D. Optical Control of Sphingosine-1-Phosphate Formation and Function. *Nat. Chem. Biol.* **2019**, *15* (6), 623.
(15) Morstein, J.; Dacheux, M. A.; Norman, D. D.; Shemet, A.; Donthamsetti, P. C.; Citir, M.; Frank, J. A.; Schultz, C.; Isacoff, E. Y.; Parrill, A. L.; Tigyi, G. J.; Trauner, D. Optical Control of Lysophosphatidic Acid Signaling. *J. Am. Chem. Soc.* **2020**, *142* (24), 10612−10616.
(16) Frank, J. A.; Moroni, M.; Moshourab, R.; Sumser, M.; Lewin, G. R.; Trauner, D. Photoswitchable Fatty Acids Enable Optical Control of TRPV1. *Nat. Commun.* **2015**, *6*, 7118.
(17) Lichtenegger, M.; Tiapko, O.; Svobodova, B.; Stockner, T.; Glasnov, T. N.; Schreibmayer, W.; Platzer, D.; de la Cruz, G. G.; Krenn, S.; Schober, R.; Shrestha, N.; Schindl, R.; Romanin, C.; Groschner, K. An Optically Controlled Probe Identifies Lipid-Gating Fenestrations within the TRPC3 Channel. *Nat. Chem. Biol.* **2018**, *14* (4), 396−404.
(18) Leinders-Zufall, T.; Storch, U.; Bleymehl, K.; Schnitzler, M. M. y; Frank, J. A.; Konrad, D. B.; Trauner, D.; Gudermann, T.; Zufall, F. PhoDAGs Enable Optical Control of Diacylglycerol-Sensitive Transient Receptor Potential Channels. *Cell Chem. Biol.* **2018**, *25* (2), 215−223.
(19) Frank, J. A.; Yushchenko, D. A.; Hodson, D. J.; Lipstein, N.; Nagpal, J.; Rutter, G. A.; Rhee, J.-S.; Gottschalk, A.; Brose, N.; Schultz, C.; Trauner, D. Photoswitchable Diacylglycerols Enable Optical Control of Protein Kinase C. *Nat. Chem. Biol.* **2016**, *12* (9), 755−762.
(20) Kol, M.; Williams, B.; Toombs-Ruane, H.; Franquelim, H. G.; Korneev, S.; Schroeer, C.; Schwille, P.; Trauner, D.; Holthuis, J. C.; Frank, J. A. Optical Manipulation of Sphingolipid Biosynthesis Using Photoswitchable Ceramides. *eLife* **2019**, *8*, No. e43230.
(21) Morstein, J.; Kol, M.; Novak, A. J. E.; Feng, S.; Khayyo, S.; Hinnah, K.; Li-Purcell, N.; Pan, G.; Williams, B. M.; Riezman, H.; Atilla-Gokcumen, G. E.; Holthuis, J. C. M.; Trauner, D. Short Photoswitchable Ceramides Enable Optical Control of Apoptosis. *ACS Chem. Biol.* **2021**, *16* (3), 452−456.
(22) Tei, R.; Morstein, J.; Shemet, A.; Trauner, D.; Baskin, J. M. Optical Control of Phosphatidic Acid Signaling. *ACS Cent. Sci.* **2021**, *7* (7), 1205−1215.
(23) Morstein, J.; Trads, J. B.; Hinnah, K.; Willems, S.; Barber, D. M.; Trauner, M.; Merk, D.; Trauner, D. Optical Control of the Nuclear Bile Acid Receptor FXR with a Photohormone. *Chem. Sci.* **2020**, *11* (2), 429−434.
(24) Hinnah, K.; Willems, S.; Morstein, J.; Heering, J.; Hartrampf, F. W. W.; Broichhagen, J.; Leippe, P.; Merk, D.; Trauner, D. Photohormones Enable Optical Control of the Peroxisome Proliferator-Activated Receptor $\gamma$ (PPAR$\gamma$). *J. Med. Chem.* **2020**, *63* (19), 10908−10920.
(25) Hartrampf, N.; Seki, T.; Baumann, A.; Watson, P.; Vepřek, N. A.; Hetzler, B. E.; Hoffmann-Röder, A.; Tsuji, M.; Trauner, D. Optical Control of Cytokine Production Using Photoswitchable Galactosylceramides. *Chem. - Eur. J.* **2020**, *26* (20), 4476−4479.
(26) Pernpeintner, C.; Frank, J. A.; Urban, P.; Roeske, C. R.; Pritzl, S. D.; Trauner, D.; Lohmüller, T. Light-Controlled Membrane Mechanics and Shape Transitions of Photoswitchable Lipid Vesicles. *Langmuir* **2017**, *33* (16), 4083−4089.
(27) Doroudgar, M.; Morstein, J.; Becker-Baldus, J.; Trauner, D.; Glaubitz, C. How Photoswitchable Lipids Affect the Order and Dynamics of Lipid Bilayers and Embedded Proteins. *J. Am. Chem. Soc.* **2021**, *143* (25), 9515−9528.
(28) Chander, N.; Morstein, J.; Bolten, J. S.; Shemet, A.; Cullis, P. R.; Trauner, D.; Witzigmann, D. Optimized Photoactivatable Lipid Nanoparticles Enable Red Light Triggered Drug Release. *Small* **2021**, *17* (21), 2008198.
(29) Jiménez-Rojo, N.; Feng, S.; Morstein, J.; Pritzl, S. D.; Harayama, T.; Asaro, A.; Vepřek, N. A.; Arp, C. J.; Reynders, M.; Novak, A. J. E.; Kanshin, E.; Ueberheide, B.; Lohmüller, T.; Riezman, H.; Trauner, D. Optical Control of Membrane Fluidity Modulates Protein Secretion. *bioRxiv* **2022**, DOI: 10.1101/2022.02.14.480333.
(30) Subramanian, T.; Pais, J. E.; Liu, S.; Troutman, J. M.; Suzuki, Y.; Leela Subramanian, K.; Fierke, C. A.; Andres, D. A.; Spielmann, H. P. Farnesyl Diphosphate Analogues with Aryl Moieties Are Efficient Alternate Substrates for Protein Farnesyltransferase. *Biochemistry* **2012**, *51* (41), 8307−8319.
(31) Broichhagen, J.; Frank, J. A.; Trauner, D. A Roadmap to Success in Photopharmacology. *Acc. Chem. Res.* **2015**, *48* (7), 1947−1960.
(32) Morstein, J.; Awale, M.; Reymond, J.-L.; Trauner, D. Mapping the Azolog Space Enables the Optical Control of New Biological Targets. *ACS Cent. Sci.* **2019**, *5* (4), 607−618.
(33) Appel, R. Tertiary Phosphane/Tetrachloromethane, a Versatile Reagent for Chlorination, Dehydration, and P−N Linkage. *Angew. Chem., Int. Ed. Engl.* **1975**, *14* (12), 801−811.
(34) Baeyer, A. Nitrosobenzol Und Nitrosonaphtalin. *Berichte Dtsch. Chem. Ges.* **1874**, *7* (2), 1638−1640.
(35) Mills, C. XCIII.—Some New Azo-Compounds. *J. Chem. Soc. Trans.* **1895**, *67* (0), 925−933.

(36) Dolence, J. M.; Poulter, C. D. A Mechanism for Posttranslational Modifications of Proteins by Yeast Protein Farnesyltransferase. *Proc. Natl. Acad. Sci. U. S. A.* **1995**, *92* (11), 5008−5011.
(37) Dolence, J. M.; Cassidy, P. B.; Mathis, J. R.; Poulter, C. D. Yeast Protein Farnesyltransferase: Steady-State Kinetic Studies of Substrate Binding. *Biochemistry* **1995**, *34* (51), 16687−16694.
(38) Pompliano, D. L.; Rands, E.; Schaber, M. D.; Mosser, S. D.; Anthony, N. J.; Gibbs, J. B. Steady-State Kinetic Mechanism of Ras Farnesyl:Protein Transferase. *Biochemistry* **1992**, *31* (15), 3800−3807.
(39) Anderegg, R. J.; Betz, R.; Carr, S. A.; Crabb, J. W.; Duntze, W. Structure of Saccharomyces Cerevisiae Mating Hormone A-Factor. Identification of S-Farnesyl Cysteine as a Structural Component. *J. Biol. Chem.* **1988**, *263* (34), 18236−18240.
(40) Diaz-Rodriguez, V.; Distefano, M. D. A-Factor: A Chemical Biology Tool for the Study of Protein Prenylation. *Curr. Top. Pept. Protein Res.* **2017**, *18*, 133−151.
(41) Diaz-Rodriguez, V.; Mullen, D. G.; Ganusova, E.; Becker, J. M.; Distefano, M. D. Synthesis of Peptides Containing C-Terminal Methyl Esters Using Trityl Side-Chain Anchoring: Application to the Synthesis of a-Factor and a-Factor Analogs. *Org. Lett.* **2012**, *14* (22), 5648−5651.
(42) Diaz-Rodriguez, V.; Hsu, E.-T.; Ganusova, E.; Werst, E. R.; Becker, J. M.; Hrycyna, C. A.; Distefano, M. D. A-Factor Analogues Containing Alkyne- and Azide-Functionalized Isoprenoids Are Efficiently Enzymatically Processed and Retain Wild-Type Bioactivity. *Bioconjugate Chem.* **2018**, *29* (2), 316−323.
(43) Marcus, S.; Caldwell, G. A.; Miller, D.; Xue, C. B.; Naider, F.; Becker, J. M. Significance of C-Terminal Cysteine Modifications to the Biological Activity of the Saccharomyces Cerevisiae a-Factor Mating Pheromone. *Mol. Cell. Biol.* **1991**, *11* (7), 3603−3612.
(44) Bader, T. K.; Rappe, T. M.; Veglia, G.; Distefano, M. D. Synthesis and NMR Characterization of the Prenylated Peptide, a-Factor. In *Biological NMR Part A*; Wand, A. J., Ed.; Methods in Enzymology; Academic Press, 2019; Vol. *614*, Chapter Eight, pp 207−238; DOI: 10.1016/bs.mie.2018.09.025.
(45) Diaz-Rodriguez, V.; Ganusova, E.; Rappe, T. M.; Becker, J. M.; Distefano, M. D. Synthesis of Peptides Containing C-Terminal Esters Using Trityl Side-Chain Anchoring: Applications to the Synthesis of C-Terminal Ester Analogs of the Saccharomyces Cerevisiae Mating Pheromone a-Factor. *J. Org. Chem.* **2015**, *80* (22), 11266−11274.
(46) Yang, C. C.; Marlowe, C. K.; Kania, R. Efficient Method for Regioselective Isoprenylation of Cysteine Thiols in Unprotected Peptides. *J. Am. Chem. Soc.* **1991**, *113* (8), 3177−3178.
(47) Yang, C. C.; Marlowe, C. K.; Kania, R. Efficient Method for Regioselective Isoprenylation of Cysteine Thiols in Unprotected Peptides. *J. Am. Chem. Soc.* **1991**, *113* (8), 3177−3178.
(48) Wollack, J. W.; Zeliadt, N. A.; Ochocki, J. D.; Mullen, D. G.; Barany, G.; Wattenberg, E. V.; Distefano, M. D. Investigation of the Sequence and Length Dependence for Cell-Penetrating Prenylated Peptides. *Bioorg. Med. Chem. Lett.* **2010**, *20* (1), 161−163.
(49) Borowiak, M.; Nahaboo, W.; Reynders, M.; Nekolla, K.; Jalinot, P.; Hasserodt, J.; Rehberg, M.; Delattre, M.; Zahler, S.; Vollmar, A.; Trauner, D.; Thorn-Seshold, O. Photoswitchable Inhibitors of Microtubule Dynamics Optically Control Mitosis and Cell Death. *Cell* **2015**, *162* (2), 403−411.
(50) Morstein, J.; Trauner, D. Photopharmacological Control of Lipid Function. In *Chemical Tools for Imaging, Manipulating, and Tracking Biological Systems: Diverse Methods for Prokaryotic and Eukaryotic Systems*; Chenoweth, D. M., Ed.; Methods in Enzymology; Academic Press, 2020; Vol. *638*, Chapter Eleven, pp 219−232; DOI: 10.1016/bs.mie.2020.04.025.
(51) Nijbroek, G. L.; Michaelis, S. Functional Assays for Analysis of Yeast Ste6Mutants. *Methods Enzymol.* **1998**, *292*, 193−212.
(52) Morstein, J.; Impastato, A. C.; Trauner, D. Photoswitchable Lipids. *ChemBioChem* **2021**, *22* (1), 73−83.
(53) Hancock, J. F.; Cadwallader, K.; Marshall, C. J. Methylation and Proteolysis Are Essential for Efficient Membrane Binding of Prenylated P21K-Ras(B). *EMBO J.* **1991**, *10* (3), 641−646.
(54) Wright, L. P.; Philips, M. R. Thematic Review Series: Lipid Posttranslational Modifications. CAAX Modification and Membrane Targeting of Ras. *J. Lipid Res.* **2006**, *47* (5), 883−891.
(55) Mullard, A. Finding the Way with LIPID MAPS. *Nat. Rev. Mol. Cell Biol.* **2008**, *9* (2), 92−92.
(56) O'Donnell, V. B.; Dennis, E. A.; Wakelam, M. J. O.; Subramaniam, S. LIPID MAPS: Serving the next Generation of Lipid Researchers with Tools, Resources, Data, and Training. *Sci. Signal.* **2019**, *12* (563), No. eaaw2964.
(57) Pearce, B. C.; Parker, R. A.; Deason, M. E.; Qureshi, A. A.; Wright, J. J. Hypocholesterolemic Activity of Synthetic and Natural Tocotrienols. *J. Med. Chem.* **1992**, *35* (20), 3595−3606.
(58) Nachnani, R.; Raup-Konsavage, W. M.; Vrana, K. E. The Pharmacological Case for Cannabigerol. *J. Pharmacol. Exp. Ther.* **2021**, *376* (2), 204−212.
(59) Ostash, B.; Walker, S. Moenomycin Family Antibiotics: Chemical Synthesis, Biosynthesis, and Biological Activity. *Nat. Prod. Rep.* **2010**, *27* (11), 1594−1617.
(60) Fiorito, S.; Preziuso, F.; Sharifi-Rad, M.; Marchetti, L.; Epifano, F.; Genovese, S. Auraptene and Umbelliprenin: A Review on Their Latest Literature Acquisitions. *Phytochem. Rev.* **2022**, *21*, 317.
(61) Furuse, J.; Kurata, T.; Okano, N.; Fujisaka, Y.; Naruge, D.; Shimizu, T.; Kitamura, H.; Iwasa, T.; Nagashima, F.; Nakagawa, K. An Early Clinical Trial of Salirasib, an Oral RAS Inhibitor, in Japanese Patients with Relapsed/Refractory Solid Tumors. *Cancer Chemother. Pharmacol.* **2018**, *82* (3), 511−519.
(62) Rotblat, B.; Ehrlich, M.; Haklai, R.; Kloog, Y. The Ras Inhibitor Farnesylthiosalicylic Acid (Salirasib) Disrupts The Spatiotemporal Localization Of Active Ras: A Potential Treatment For Cancer. In *Small GTPases in Disease, Part B*; Balch, W. E., Der, C. J., Hall, A., Eds.; Methods in Enzymology; Academic Press, 2008; Vol. *439*, pp 467−489; DOI: 10.1016/S0076-6879(07)00432-6.
(63) Mayer, M. P.; Prestwich, G. D.; Dolence, J. M.; Bond, P. D.; Wu, H. Y.; Poulter, C. D. Protein Farnesyltransferase: Production in Escherichia Coli and Immunoaffinity Purification of the Heterodimer from Saccharomyces Cerevisiae. *Gene* **1993**, *132* (1), 41−47.
(64) Gaon, I.; Turek, T. C.; Weller, V. A.; Edelstein, R. L.; Singh, S. K.; Distefano, M. D. Photoactive Analogs of Farnesyl Pyrophosphate Containing Benzoylbenzoate Esters: Synthesis and Application to Photoaffinity Labeling of Yeast Protein Farnesyltransferase. *J. Org. Chem.* **1996**, *61* (22), 7738−7745.
(65) Gangopadhyay, S. A.; Losito, E. L.; Hougland, J. L. Targeted Reengineering of Protein Geranylgeranyltransferase Type I Selectivity Functionally Implicates Active-Site Residues in Protein-Substrate Recognition. *Biochemistry* **2014**, *53* (2), 434−446.
(66) Blanden, M. J.; Suazo, K. F.; Hildebrandt, E. R.; Hardgrove, D. S.; Patel, M.; Saunders, W. P.; Distefano, M. D.; Schmidt, W. K.; Hougland, J. L. Efficient Farnesylation of an Extended C-Terminal C(x)3X Sequence Motif Expands the Scope of the Prenylated Proteome. *J. Biol. Chem.* **2018**, *293* (8), 2770−2785.
(67) Anderson, J. L.; Frase, H.; Michaelis, S.; Hrycyna, C. A. Purification, Functional Reconstitution, and Characterization of the Saccharomyces Cerevisiae Isoprenylcysteine Carboxylmethyltransferase Ste14p. *J. Biol. Chem.* **2005**, *280* (8), 7336−7345.
(68) Coffinier, C.; Hudon, S. E.; Farber, E. A.; Chang, S. Y.; Hrycyna, C. A.; Young, S. G.; Fong, L. G. HIV Protease Inhibitors Block the Zinc Metalloproteinase ZMPSTE24 and Lead to an Accumulation of Prelamin A in Cells. *Proc. Natl. Acad. Sci. U. S. A.* **2007**, *104* (33), 13432−13437.


https://doi.org/10.1021/acschembio.2c00645
ACS Chem. Biol. 2022, 17, 2945−2953